

On the depinning of a drop of partially wetting liquid on a rotating cylinder

Uwe Thiele

Department of Mathematical Sciences,

Loughborough University, Leicestershire LE11 3TU, UK

We discuss the analogy of the behaviour of films and drops of liquid on a rotating horizontal cylinder on the one hand and substrates with regular one-dimensional wettability patterns on the other hand. Based on the similarity between the respective governing long-wave equations we show that a drop of partially wetting liquid on a rotating cylinder undergoes a depinning transition when the rotation speed is increased. The transition occurs via a snipe bifurcation as in a recently described scenario for drops depinning on heterogeneous substrates.

The manuscript was accepted by the *J. Fluid Mech.* in October 2010 and will be published in the following months.

I. INTRODUCTION

Motivated by the question how much honey can be kept on a breakfast knife by rotating the knife about its long axis, Moffatt studied the destabilisation of a film on the outside of a rotating horizontal cylinder and the subsequent development of regular patterns of azimuthal rings [29]. He also gives a lubrication equation that incorporates gravity and viscosity effects but neglects surface tension and inertia. It is based on a model by [40] which includes surface tension. Related questions had been studied before by [56] employing a rotating horizontal cylinder which is at the bottom immersed in a liquid bath. i.e., in contrast to [29] the amount of liquid on the cylinder is not an independent control parameter. The related case of a liquid film covering the inner wall of a horizontal rotating cylinder was first studied by [37] who discussed experiments performed with water employing an inviscid model incorporating gravitational and centrifugal forces.

Since the early experimental results engineers and scientists alike have studied flows of

free-surface films of liquid on the inner or outer wall of resting or rotating horizontal cylinders in a number of different settings. The studied systems are of high importance for several coating and printing processes where rotating cylinders transport the coating material in the form of liquid films. In the present contribution we will discuss the analogy between film flow and drop motion on a rotating horizontal cylinder on the one hand and on heterogeneous substrates with regular wettability patterns on the other hand. First, however, we will give a short account of the seemingly disconnected fields.

The theoretical analyses given by [56] and [37] for the flow on/in a rotating cylinder were based on linear stability considerations based on the full hydrodynamic equations for momentum transport, i.e., the Navier-Stokes equations. Their studies were extended later on, e.g., by [35] who considered inviscid film flow on the in- and outside of the cylinder in a unified manner, and [45] whose analysis includes viscous film flow at small and large Reynolds numbers.

However, most analyses of the non-linear behaviour are based on a long-wave or lubrication approximation [33] valid for the case where the thickness of the liquid film $h(\theta, t)$ is small as compared to the radius of the cylinder R . The resulting evolution equation for the film thickness profile

$$\partial_t h = -\partial_\theta \left\{ h^3 [\tilde{\alpha} \partial_\theta (\partial_{\theta\theta} h + h) - \tilde{\gamma} \cos(\theta)] + h \right\} \quad (1)$$

was first given by [40] and used by [29] (without capillarity effects, i.e., $\tilde{\alpha} = 0$). In the dimensionless Eq. (1), $\tilde{\alpha} = 3\varepsilon^3\sigma/R\omega\tilde{\eta}$ and $\tilde{\gamma} = \varepsilon^2\rho gR/3\omega\tilde{\eta}$ are the scaled dimensionless surface-tension and gravity parameter, respectively [18]. It is important to note that both depend on the angular velocity of the rotation ω , the dynamic viscosity $\tilde{\eta}$, the cylinder radius R , and the ratio ε of mean film thickness \bar{h} and R . The remaining material constants are surface tension σ and density ρ , and g is the gravitational acceleration. The angle θ determines the position on the cylinder surface and is measured anti-clockwise starting at the horizontal position on the right. The force $\tilde{\gamma} \cos(\theta)$ corresponds to the component of gravity parallel to the cylinder surface.

The long-wave equation (1) including surface tension effects has been studied in detail by, e.g., [18, 41] and [23]. Note that for the parameter ranges where Eq. (1) applies, it is valid without difference for films on the outside and inside of the cylinder (cf., e.g., [2, 18, 31]). A preliminary comparison of the long-wave approach to results obtained with the Stokes

equation is given by [36]. Various extensions of Eq. (1) were developed. See, in particular, [1] for a discussion of hydrostatic effects. Other higher order terms related to gravity, inertial and centrifugal effects have been included [2, 8, 14, 15, 19, 25, 31, 32]. In particular, [31] and [25] present a systematic derivation of several such higher order models and give also detailed comparisons to a number of previous studies as e.g., [32], [2] and [8]. The film stability and non-linear evolution of a film on the outside of a non-isothermal horizontal cylinder was considered without [43] and with [13] rotation. Most of the aforementioned studies consider two-dimensional situations. The fully three-dimensional problem is studied for the cases without [55] and with [15, 30] rotation.

The second system that we would like to discuss are liquid drops and films on heterogeneous solid substrates as studied experimentally, e.g. by [46] and [42]. Although in principle the heterogeneity may result from substrate topography or chemical heterogeneities we focus here on the case of a smooth flat substrate with chemical heterogeneities, i.e., we assume the substrate wettability depends on position. Horizontal heterogeneous substrates are often considered in connection with micro-patterning of soft matter films via thin film dewetting [3, 11, 26, 44]. Another application are free-surface liquid channels in microfluidics [16]. Often one employs thin film evolution equations obtained through a long-wave approximation to study the dynamics of dewetting for an initially flat film or to analyse steady drop and ridge solutions and their stability on such patterned substrates (see, e.g., [24] and [49]). Static structures may also be studied using a variational approach [10, 27].

More recently a model system was introduced to study the dynamics of drops on heterogeneous inclined substrates. The models apply also to such drops under other driving forces along the substrate [52]. The corresponding dimensionless evolution equation for the one-dimensional film thickness profile (i.e., describing a two-dimensional drop) is of the form

$$\partial_t h = -\partial_x \left\{ h^3 [\partial_x (\partial_{xx} h + \Pi(h, x))] + \tilde{\mu} \right\}, \quad (2)$$

where $\tilde{\mu}(h)$ represents the lateral driving force (μh^3 in the case of an inclined substrate, where μ is the inclination angle). The position-dependent disjoining pressure $\Pi(h, x)$ models the heterogeneous wettability of the substrate. One notices at once that Eqs. (2) and (1) are rather similar: Identifying $x = \theta$, $\tilde{\mu}(h) = h$ and $\Pi(h, x) = \tilde{\alpha}h - \tilde{\gamma}\sin(x)$, Eq. (1) may for $\tilde{\alpha} = 1$ be seen as a special case of Eq. (2). Here, we use the analogy to study drops or films on a rotating cylinder. In particular, we show that drops on a rotating cylinder may show

rather involved depinning dynamics analogous to the behaviour of drops on heterogeneous substrates [5, 51, 52].

To illustrate the behaviour we choose the case of drops of a partially wetting liquid on a substrate with a periodic array of localised hydrophobic wettability defects [52]. On a horizontal substrate one finds steady drops that are positioned exactly between adjacent defects, i.e., the drops stay on the most wettable part. At a small lateral driving force μ the $x \rightarrow -x$ symmetry of the system is broken. However, the drops do not slide continuously along the substrate as they do in the case of a substrate without defects [53]. Their advancing contact line is blocked by the next hydrophobic defect, i.e., one finds steady pinned drops at an upstream position close to the defect. As the driving force is increased, the drops are pressed further against the defect. As a result the steady drops steepen. At a finite critical value μ_c the driving force allows the drop to overcome the adverse wettability gradient and the drop depins from the defect and begins to slide. In a large part of the parameter space spanned by the wettability contrast and the drop size the point of depinning at μ_c corresponds to a Saddle-Node Infinite PERiod (sniper) bifurcation. Beyond μ_c the drops do not slide continuously down the incline. They rather perform a stick-slip motion from defect to defect [51, 52]. However, in another region of the parameter space the depinning can occur via a Hopf bifurcation, i.e., with a finite frequency. In particular, this happens in the case of rather thick wetting layers.

The aim of the present contribution is to elucidate under which conditions a similarly intricate ‘depinning’ behaviour can be found for a pendant drop underneath a horizontal cylinder when increasing the speed of rotation. In the following section II we will discuss our scaling and introduce a long-wave model for a film of partially wetting liquid on a rotating cylinder. It allows (even without gravitation) for the coexistence of drops and a wetting layer. We discuss several physical situations it can be applied to. Next, section III presents steady state solutions depending on the non-dimensional rotation velocity for several thicknesses of the wetting layer and discusses the depinning scenario in the case of the partially wetting liquid. Finally, we conclude and give an outlook in Section IV.

II. MODEL

Before we introduce our long-wave model we discuss our scales. In the non-dimensionalisation used in most works studying Eq. (1) the angular velocity of the cylinder rotation ω is not reflected in a single dimensionless parameter but both dimensionless parameters are inversely proportional to ω . Furthermore, the time scale depends on ω [18, 40]. This and a further re-scaling of the equation for steady drop and film states, that absorbs the flow rate into both dimensionless parameters and also into the thickness scale, implies that the existence of two steady solutions for identical parameters (thin capillary film and pendant drop with through-flow), shown analytically by [41] and numerically by [23], actually refers to solutions of different liquid volume.

Such a scaling is not convenient for our study as we would like to investigate the change in system behaviour for fixed liquid volume when increasing the rotation speed of the cylinder from zero, i.e., ω should only enter a single dimensionless parameter that will be our main control parameter. A scaling fit for our purpose is the one based on the scales of the gravity-driven drainage flow employed by [14].

Note also that in particular [23] and to a lesser extent [55] represent some of their solutions in a way that misrepresents their findings and, in general, the concept of an equation in long-wave approximation. Whenever one shows the solutions as a thickness profile on a cylinder one has to pick a particular radius R and smallness ratio ϵ for the representation (cf. Figs. 3, 5 and 9 below). This is a rather arbitrary choice as the equation in long-wave approximation is strictly valid only in the limit $\epsilon \rightarrow 0$, i.e. it is always only an approximation to a real physical situation where ϵ is finite.

In the present work we focus on solutions without axial variation, i.e., we consider the two-dimensional physical situation depicted in Fig. 1. Following [14] we use \bar{h} , R , $\rho g \bar{h}^2 / \eta$, $\epsilon \rho g \bar{h}^2 / \eta$, $3\eta / \epsilon \bar{h} \rho g$ and $\rho g \bar{h}$ to scale the coordinate z orthogonal to the cylinder surface, the coordinate $x = \theta R$ along the surface, the two velocity components v_x and v_z , time, and pressure, respectively. The ratio of z - and x -scale is the smallness parameter $\epsilon = \bar{h} / R$, i.e., the film height is scaled by $\bar{h} = \epsilon R$. Here the angle θ is defined in clockwise direction starting at the upper vertical position, i.e., a pendant droplet underneath the resting horizontal cylinder has its centre of mass at $\theta = \pi$.

The evolution equation is derived from the Navier-Stokes equations with no-slip boundary

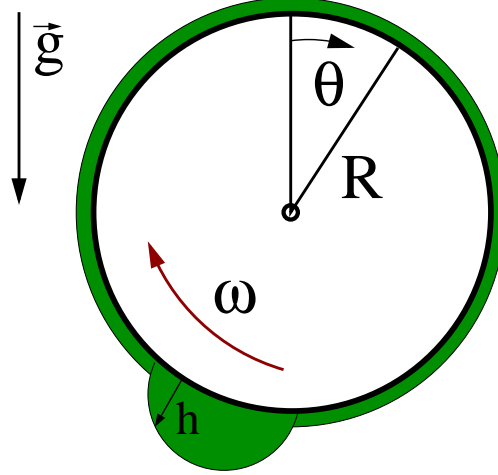


FIG. 1: Sketch of a drop of partially wetting liquid coexisting with a thick wetting layer on a rotating cylinder.

conditions at the (rotating) cylinder, and tangent- and normal force equilibria at the free surface using the long-wave approximation [14, 33, 40, 43]. Note that here we furthermore assume that the ratio \bar{h}/R and the physical equilibrium contact angle are both of $O(\varepsilon)$ (cf. Section IV). This gives

$$\partial_\tau h = -\partial_\theta \left\{ h^3 \partial_\theta \left[\text{Bo}^{-1} (\partial_{\theta\theta} h + h) - \cos(\theta) + \tilde{\Pi}(h) \right] + \tilde{\Omega} h \right\}, \quad (3)$$

where τ is the non-dimensional time, and

$$\text{Bo} = \frac{R^3 \rho g}{\bar{h} \sigma} \quad \text{and} \quad \tilde{\Omega} = \frac{\eta \omega R}{\rho \bar{h}^2 g} \geq 0 \quad (4)$$

are an effective Bond number and a rotation number for a clock-wise rotation, respectively. The latter corresponds to the ratio of the rotation velocity at the cylinder surface and the drainage velocity. The function $\tilde{\Pi}(h)$ is a non-dimensional disjoining pressure that accounts for the wettability of the liquid film on the cylinder surface [9, 17, 21].

To make the analogy with the depinning droplet on a heterogeneous substrate more obvious we introduce another timescale $t = \tau/\text{Bo}$, disjoining pressure $\Pi = \text{Bo} \tilde{\Pi}$ and rotation number $\Omega = \text{Bo} \tilde{\Omega}$ and obtain

$$\partial_t h = -\partial_\theta \left\{ h^3 \partial_\theta \left[\partial_{\theta\theta} h + h - \text{Bo} \cos(\theta) + \Pi(h) \right] + \Omega h \right\}, \quad (5)$$

with

$$\Omega = \frac{\eta \omega R}{\varepsilon^3 \sigma}. \quad (6)$$

Defining the derivative

$$\partial_h f = -\Pi(h) - h + \text{Bo} \cos(\theta) \quad (7)$$

of a ‘local free energy’ $f(h, \theta)$ and identifying $\tilde{\mu} = \Omega h$, Eq. (5) takes the form of Eq. (2) and the Bond number takes the role of a ‘heterogeneity strength’. Note that the scaling used is well adapted for discussing independently the influences of rotation and gravity in the presence of capillarity. However, it does not allow for a study of the limit of vanishing surface tension.

As disjoining pressure we choose here the combination of a long- and a short-range power law $\Pi(h) = \text{Ha}/h^3 (1 - b/h^3)$, where Ha is a dimensionless Hamacker constant. For $b > 0$ one has a precursor film or wetting layer thickness $h_0 = b^{1/3}$ [38, 39, 48]. This is valid only for $\text{Ha} < 0$, i.e., when the long-range interaction is destabilising. This corresponds to the case of a partially wetting liquid. For $\text{Ha} > 0$, a rather thick wetting layer can be stabilised and the b/h^6 term is of no further relevance and could just as well be dropped.

Note that $\partial_h f$ may contain other terms beside the ones in Eq. (7). For a heated or cooled cylinder a term $(3/2) \text{BoBiMa} \log[h/(1 + \text{Bi} h)] + 1/(1 + \text{Bi} h)$ would enter where Bi is the Biot number and Ma an effective Marangoni number [34, 43, 50]. If the rotating cylinder forms the inner electrode of a cylindrical capacitor, a term $\text{Vo}/[h + (d - h)\epsilon]^2$ has to be included for a dielectric liquid and DC voltage of non-dimensional strength Vo (ϵ is the electric permittivity and d the distance between the two cylinders (see appendix of [52] and [22]). The similarity in the behaviour of depinning drops under the influence of different physical effects in the case that the effective pressure terms ‘look similar’ is discussed by [52].

Although here we do not consider such other physical effects explicitly, we will explore the effect of corresponding thick wetting layers by adapting the parameters of our disjoining pressure accordingly. A thick wetting layer that coexists with droplets might, for instance, result from the interplay of a destabilising thermal or electrical effect and a stabilising long-range van der Waals interaction. We obtain adequate values of Ha and b for our present $\Pi(h)$ by relating them to the (non-dimensional) thickness of the wetting layer h_0 and a static macroscopic contact angle β_0 by [see, e.g., 17]

$$b = h_0^3 \quad \text{and} \quad \text{Ha} = -\frac{5}{3} \beta_0^2 h_0^2. \quad (8)$$

Note, that β_0 is the angle in long-wave scaling, i.e., a small physical equilibrium contact

angle $\beta_{\text{eq}} = \varepsilon\beta_0$ corresponds to a long-wave contact angle β_0 of $O(1)$. In the limit of a non-rotating cylinder (i.e. $\Omega = 0$) and assuming the disjoining pressure corresponds to complete wetting ($\text{Ha} > 0$, $1/h^6$ term may be dropped), our equation (5) corresponds to the one given by [43] for the isothermal case. There, however, first a viscous scaling is used, which they transform in a second step – a rescaling of time and therefore velocities with the Galileo number – into the ‘drainage scaling’ used here. Our equation corresponds also to that of [18] when the disjoining pressure is added to their equation.

To analyse the system behaviour we determine in the following steady-state solutions that correspond, e.g., to pendant droplets. The behaviour beyond the depinning threshold is analysed using time-stepping algorithms. As we restrict ourselves to the two-dimensional physical situation an explicit scheme for stiff equations suffices for the latter. The steady-state solutions are obtained using the continuation techniques of the package AUTO [12]. The steady and time-periodic solutions are characterized by their L^2 norm $\|\delta h\| \equiv \sqrt{(1/2\pi) \int_0^{2\pi} (h(\theta) - 1)^2 d\theta}$ and time-averaged L^2 norm $\|\delta h\| \equiv \sqrt{(1/2\pi T) \int_0^T \int_0^{2\pi} (h(\theta) - 1)^2 d\theta dt}$, respectively. T is the time period.

Note finally that Eq. (5) is the result of our choices for the relative order of magnitude of the involved dimensionless numbers that is based on the choice of physical effects that shall be discussed (cf. [33]). Once this is accepted, equation (5) is to $O(1)$ asymptotically correct. Its form as a conservation law implies that $\int_0^{2\pi} h d\theta = 2\pi$. To $O(1)$ this corresponds to mass conservation. For a discussion of higher order corrections to this picture see [25].

III. RESULTS

A. Parameters

We base our estimate for realistic Bond and rotation numbers on two liquids typically studied in the literature: (i) water at 25°C as in [43] and a silicone oil with $\sigma = 0.021\text{N/m}$, $\eta = 1\text{kg/ms}$ and $\rho = 1200\text{kg/m}^3$ as in [14]. As experimentally feasible configurations we assume angular rotation velocities $\omega = 0.1 \dots 10\text{s}^{-1}$, cylinder of radii $R = 10^{-3} \dots 10^{-2}\text{m}$ and smallness ratios $\varepsilon = 0.01 \dots 0.1$. It is only for the purpose of illustration of steady droplets on a cylinder that we later use $\varepsilon = 0.1$ in selected figures.

For $\omega = 1\text{s}^{-1}$ and a smallness ratio $\varepsilon = 0.1$ we find for a cylinder of radius $R = 10^{-2}\text{m}$ for

material (i) $\text{Bo} = 136$ and $\Omega = 0.14$, whereas material (ii) gives $\text{Bo} = 561$ and $\Omega = 476$. For a smaller cylinder radius of $R = 10^{-3}\text{m}$ one has (i) $\text{Bo} = 1.36$ and $\Omega = 0.014$, and (ii) $\text{Bo} = 5.61$ and $\Omega = 47.6$. Decreasing the smallness ratio to $\varepsilon = 10^{-2}$ increases all Bond numbers by a factor 10 and all rotation numbers by a factor 10^3 . Focusing on cylinder diameters in the millimetre range, we mainly investigate $\text{Bo} \leq 10$. Note that experiments may also be performed with larger cylinders. To keep the Bond number in the interesting range one could decrease the relevant density by replacing the ambient gas by a second (immiscible) liquid. A feasible experimental set-up could be a horizontal Taylor-Couette apparatus with rotating inner cylinder. The theoretical framework would also need to be amended – replacing the one-layer theory [Eq. (5)] by a closed two-layer model similar to [28].

Note, that silicone oils may have viscosities 2 orders of magnitude smaller or larger than the chosen value and one is able to vary the velocity of rotation in a wide range. This implies that there is some flexibility in the choice of Ω . We will find that for $\text{Bo} = O(1)$ the interesting range for the rotation number is $\Omega = O(1)$. For instance, with $\text{Bo} = 1$ one finds that depinning occurs at $\Omega = 1.68$.

As the present work aims at establishing the qualitative correspondence between the behaviour of a depinning drop on a heterogeneous substrate and the one of a droplet on a rotating cylinder we restrict our results to one partially wetting case (choosing $h_0 = 0.1$ and $\beta_0 = 2$) and the completely wetting case ($\beta_0 = 0$). For comparison, selected results are also shown for the contact angle $\beta_0 = 1$.

Note that here the scaling and therefore the discussion of the smallness parameter ϵ is based on $\epsilon = \bar{h}/R$, i.e., we use the ratio of mean film thickness and cylinder radius. In the case of pendant drop solutions one also has to keep the maximal film height h_{max} in mind when discussing ϵ as the scaling becomes questionable when $h_{\text{max}} \gg \bar{h}$. This is, however, normally not the case. In the present work the ratio h_{max}/\bar{h} is always below 3. Although an inspection of the figures in [23] shows a ratio h_{max}/\bar{h} that is not much larger, one notices that there ϵ itself (based on \bar{h}) seems to be larger than one (see remark above Eq. (II)). The same applies to Fig. 3 of [55]. There exists no such problem in the region where only a thin wetting layer of thickness h_{min} covers the cylinder even if $h_{\text{min}} \ll \bar{h}$. Actually, the long-wave approximation gets better there. In an approach based on matched asymptotics one could further simplify the governing equation in this region (cf. [7]). However, such an approach is not taken here as it is of limited use when considering parameter regions that

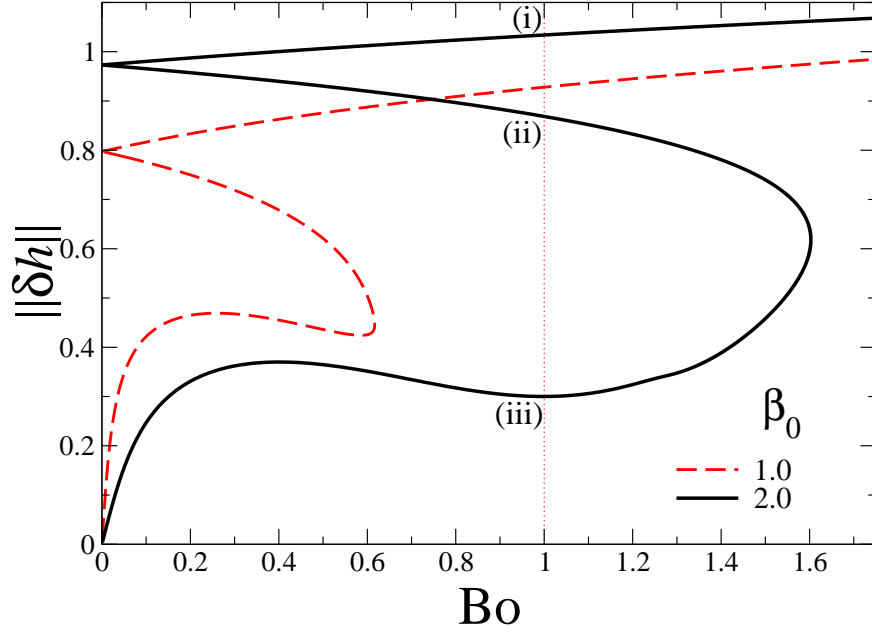


FIG. 2: Solutions on a horizontal cylinder without rotation ($\Omega = 0$) are characterised by their L^2 norm as a function of the Bond number for two different equilibrium contact angles β_0 and $h_0 = 0.1$, $\bar{h} = 1.0$.

show qualitative changes in solution behaviour, e.g., close to the sniper bifurcation discussed below.

B. Partially wetting case

First, we consider the case of a horizontal cylinder without rotation ($\Omega = 0$) and determine steady drop and film solutions. Employing the Bond number as control parameter we obtain families of steady state solutions for two selected values of the equilibrium contact angle β_0 . Inspecting Fig. 2 one notices that above a critical value of the Bond number Bo_c there exists only a single solution. It corresponds to a symmetric pendant drop located underneath the cylinder. An example for $Bo = 1$ and $\beta_0 = 2.0$ is given as solid line in Fig. 3. However, two additional steady solutions exist below Bo_c . One of them corresponds to an unstable symmetric drop sitting on top of the cylinder (dotted line in Fig. 3). The other one corresponds to an unstable solution that has two minima – a deep one underneath the cylinder and a shallow one on top of it (dashed line in Fig. 3).

We find that Bo_c becomes smaller with decreasing contact angle β_0 , i.e., the range of Bo

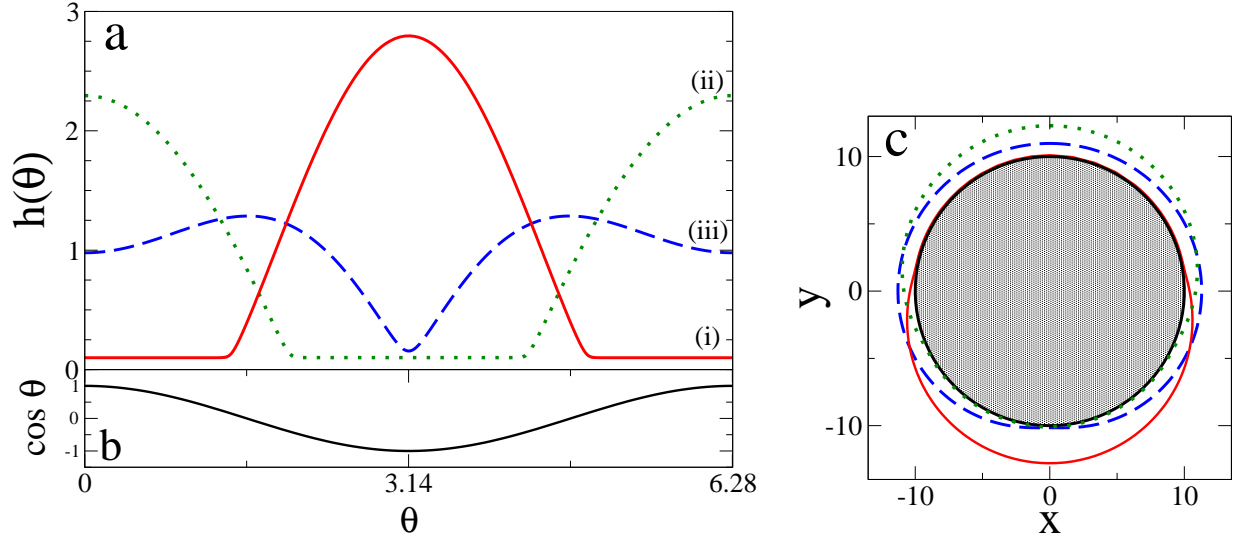


FIG. 3: Steady film thickness profiles on a horizontal cylinder without rotation ($\Omega = 0$) for $\text{Bo} = 1$ and $\beta_0 = 2.0$ (corresponding to marks (i) to (iii) in Fig. 2). The remaining parameters are as in Fig. 2. Panel (a) gives the profiles as $h(\theta)$, (b) gives the space-dependent part of $\partial_h f$ (Eq. (7)), and panel (c) shows the profiles on a cylinder. Note that for illustration purposes we have (rather arbitrarily) assumed a radius $R = 10$, i.e. $\varepsilon = 0.1$ (cf. discussion in Section III A). Line styles in (c) correspond to those in (a). The cylinder surface is represented by the solid black line.

numbers where steady structures beside the pendant drop exist becomes smaller. The completely wetting case ($\beta_0 = 0$) is qualitatively different and is discussed below in Section III C. Increasing β_0 above $\beta_0 = 2$ the critical value Bo_c strongly increases, e.g., for $\beta_0 = 10$ one finds $\text{Bo}_c = 43.3$.

Note, that the pendant drop underneath the cylinder [drop on top of cylinder] corresponds on a horizontal heterogeneous substrate to the drop on the more [less] wettable region as discussed by [49]. The limit of zero Bond number is analogue to the horizontal homogeneous substrate.

Next, we increase the dimensionless angular velocity Ω for several selected Bond numbers and determine the steady state solutions (Fig. 4). Focusing first on $\text{Bo} = 1$ we recognise at $\Omega = 0$ three solutions as marked by the vertical dotted line in Fig. 2. The curve of largest norm corresponds to the pendant drop. As Ω increases from zero, its norm and amplitude decrease slightly, whereas its centre of mass moves towards larger θ , it is ‘dragged along’ by the rotation without changing its shape much. This can be well appreciated in Fig. 5 which

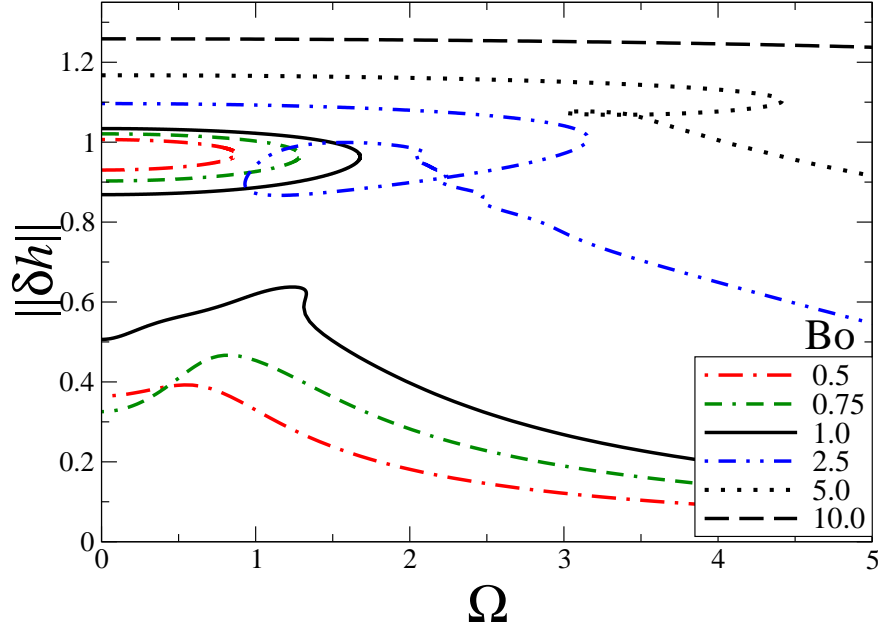


FIG. 4: Solutions on a horizontal rotating cylinder as a function of the Rotation number Ω for various Bond number Bo as given in the legend and contact angle $\beta_0 = 2.0$. The drop and film profiles are characterised by their L^2 norm. The remaining parameters are $h_0 = 0.1$, and $\bar{h} = 1.0$.

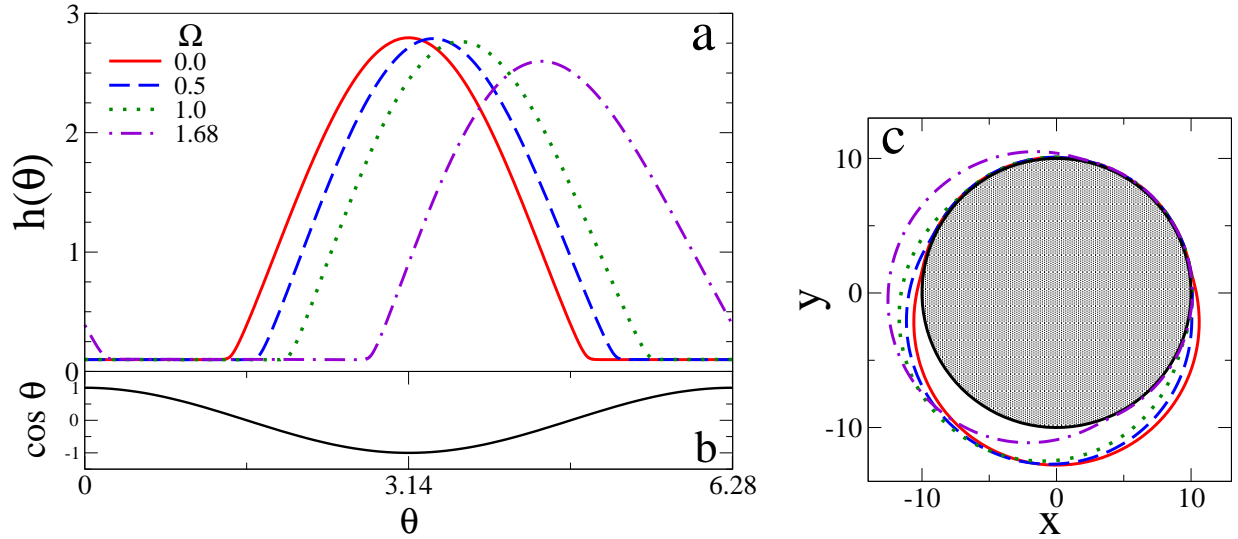


FIG. 5: Steady film thickness profiles on a rotating horizontal cylinder for Bond number $Bo=1$ and $\beta_0 = 2.0$ for Rotation numbers Ω as given in the legend. All shown solutions are situated on the stable upper branch in Fig. 4. The remaining parameters are as in Fig. 4. Panel (a) gives the profiles as $h(\theta)$, (b) gives the space-dependent part of $\partial_n f$ (Eq. (7)), and panel (c) illustrates the profiles on a cylinder assuming a radius $R = 10$. Line styles in (c) correspond to those in (a).

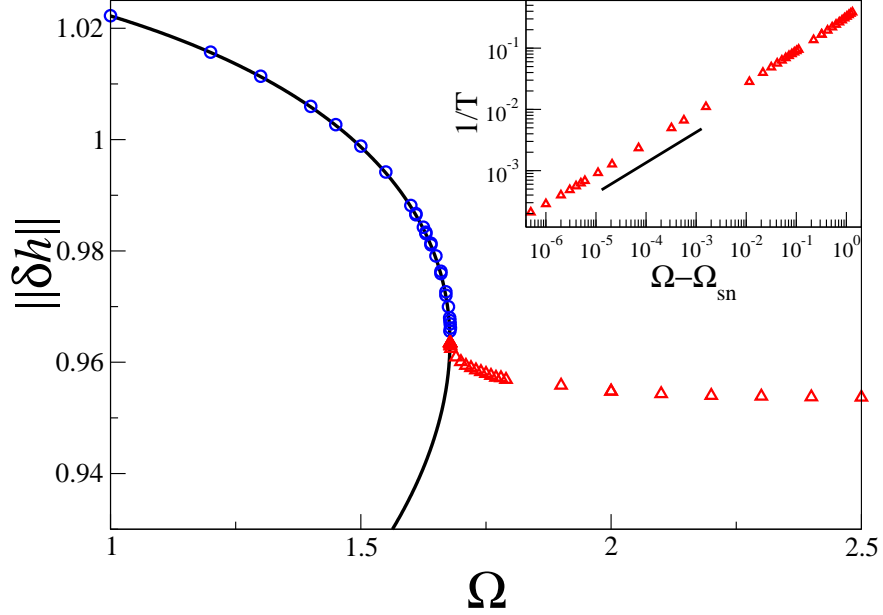


FIG. 6: Bifurcation diagram for the depinning transition for a drop on a rotating cylinder with $Bo=1$ and $\beta_0=2.0$. Shown are the L^2 norm for the branch of steady solutions as obtained by continuation (solid line), selected steady solutions as obtained by direct integration in time (circles) and the time-averaged L^2 norm for the unsteady solutions beyond the sniper depinning bifurcation (triangles). The inset gives for the latter a log-log plot of the dependence of the inverse temporal period on the distance from the bifurcation $\Omega - \Omega_{sn}$. The solid line indicates an exponent of $1/2$.

gives selected profiles for the branch of pendant drop solutions. The branch terminates in a saddle-node bifurcation at $\Omega_{sn} = 1.68$ where it annihilates with one of the unstable branches. The third branch, i.e., the one of lowest norm, shows for increasing Ω an increase in the norm, then it undergoes two saddle-node bifurcations at $\Omega = 1.313$ and $\Omega = 1.329$. At larger Ω the norm decreases again. Note that the two saddle-node bifurcations are a first sign of rather complicated re-connections which occur when one increases Bo from 1.0 to 2.5. The re-connections involve further (unstable) branches that are not shown in Fig. 4 and result in the loop structure observed for $Bo=2.5$ at about $\Omega = 1.5$. A further indication for the existence of additional branches is the observation that the value of the norm at $\Omega = 0$ for $Bo=1.0$ in Fig. 4 does not agree with the lowest norm at $Bo=1.0$ in Fig. 2. As the re-connections are not relevant for the depinning transition we will here not consider them further.

At Bond numbers smaller than $Bo=1$ the behaviour is qualitatively the same as described

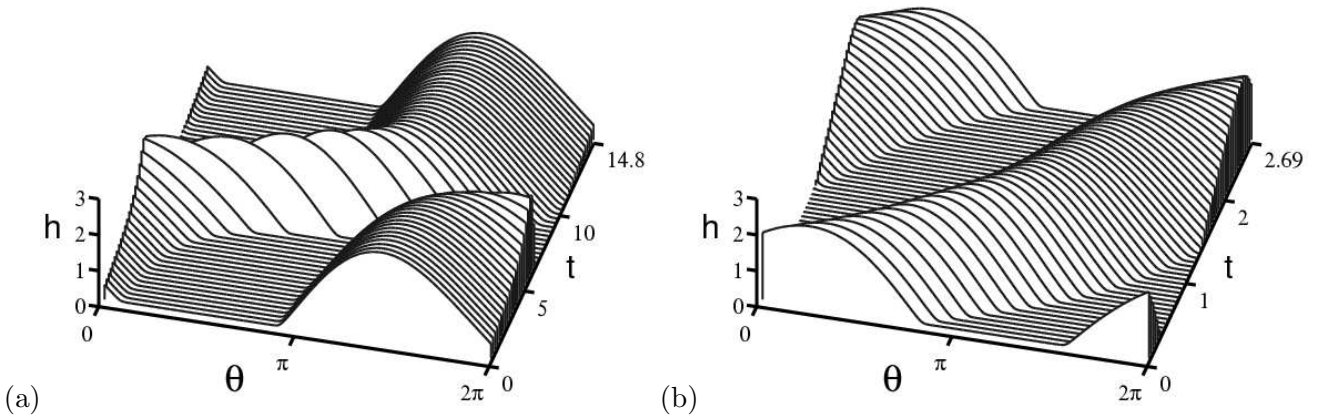


FIG. 7: Space-time plots illustrating the time evolution of co-rotating drops beyond depinning via a sniper bifurcation (at $\Omega > \Omega_{\text{sn}}$). Shown is one period in space and time (a) close to depinning at Rotation number $\Omega = 1.8$ with a temporal period of $T = 14.8$, and (b) far from depinning at $\Omega = 3.0$ with $T = 2.7$. The Bond number is $\text{Bo} = 1$ and $\beta_0 = 2.0$.

for $\text{Bo} = 1$. However, the critical Ω_{sn} becomes smaller with decreasing Bo . Above, we have discussed that the behaviour at $\Omega = 0$ changes qualitatively when decreasing Bo beyond Bo_c (Fig. 2). Although this also affects the behaviour at small Ω it has less influence on the behaviour at larger Ω (Fig. 4). In particular, the saddle-node at Ω_{sn} where the pendant drop solution ceases to exist, persists for larger Bond number as does the related dynamic behaviour (see below). Note that for $\text{Bo} = 10$ the saddle-node is at $\Omega_{\text{sn}} \approx 6.2$ outside the range of Fig. 4.

An interesting resulting question is what happens to a stable obliquely pendant droplet at $\Omega < \Omega_{\text{sn}}$ when the rotation velocity is further increased such that it is slightly larger than Ω_{sn} ? Does the solution approach the remaining steady solution? Simulations of Eq. (5) show that this is not the case. For $\Omega > \Omega_{\text{sn}}$ the droplet moves in a non-stationary way with the rotating cylinder and corresponds to a space- and time-periodic solution. The resulting bifurcation diagram for $\text{Bo} = 1$ is given in Fig. 6. It shows that the ‘new’ branch of space- and time-periodic solutions (characterised by its time-averaged norm) emerges from the saddle node bifurcation of the steady solutions at Ω_{sn} . The behaviour close to and far from the saddle-node bifurcation is illustrated in the space-time plots of Fig. 7. Panel (b) shows that far away from the bifurcation the drop moves continuously with its velocity and shape varying smoothly. It moves fastest when its maximum passes $\theta \approx \pi/2$ (velocity ≈ 4.6)

and slows down when passing $\theta \approx 3\pi/2$ (velocity ≈ 1.2), i.e., respectively, when gravity most strongly supports and hinders the motion driven by the cylinder rotation. The ratio of largest to smallest velocity is about 4:1. When approaching the bifurcation from above, the droplet still moves with the rotation but the time scales of the slow and the fast phase become very different. For instance, at $\Omega = 1.8$ (Fig. 7 (a)) the drop moves fastest when passing $\theta \approx \pi/2$ (velocity ≈ 3.3). However, when the drop is situated at about $\theta = 3\pi/2$ it barely moves (velocity ≈ 0.1) resulting in a velocity ratio of 33:1 between the fastest and slowest phase. The resulting overall behaviour strongly resembles the stick-slip motion discussed in the context of contact line motion on heterogeneous substrates [52]. Note that it also resembles so-called sloshing modes found for a partially liquid-filled rotating cylinder [19, 54].

The ratio of the velocities diverges when approaching the bifurcation point. In consequence, the frequency $1/T$ of the periodic drop motion goes to zero. As shown in the inset of Fig. 6, the dependence corresponds to a power law $1/T \sim (\Omega - \Omega_{\text{sn}})^{1/2}$. This indicates that the bifurcation at Ω_{sn} is actually a Saddle-Node-Infinite-PERiod bifurcation (or ‘sniper’ for short; see [47], and discussion by [52]).

The described behaviour is quite generic for the partially wetting case, i.e., it is found in a wide range of parameters, in particular, Bond number, contact angle and wetting layer thickness. However, the behaviour changes dramatically when strongly decreasing the contact angle, i.e., when approaching the completely wetting case.

C. The completely wetting case

After having discussed the intricate depinning behaviour in the partially wetting case, to emphasise the contrast, we consider briefly the completely wetting case ($\beta_0 = 0$). Note that the physical setting is then identical to the one employed in most studies of the classic Moffatt problem [29, 40]. However, the parametrisation used here is different and results in Eq. (5) with $\text{Ha} = 0$. We analyse the system behaviour as above by studying the steady state solutions without and with rotation.

In the case without rotation, the first difference one notices is that for fixed Bond number only one solution exists. It corresponds to the pendant drop solution. With increasing Bo , i.e., with increasing importance of gravity, its amplitude monotonically increases. Fixing

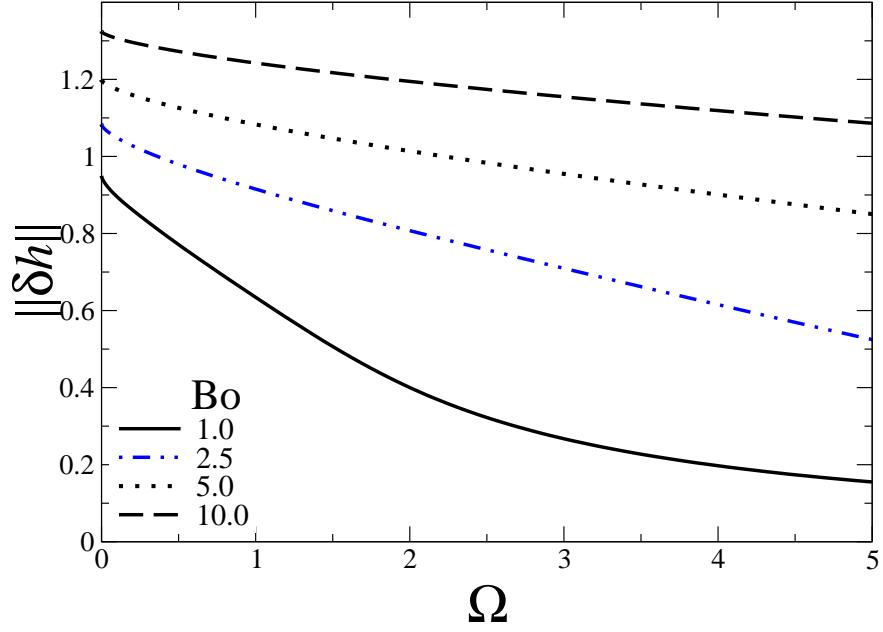


FIG. 8: Solutions for a film of completely wetting fluid ($\beta_0 = 0$) on a horizontal rotating cylinder as a function of the Rotation number Ω for various Bond numbers Bo as given in the legend. The solutions are characterised by their L^2 norm. The remaining parameter is $\bar{h} = 1.0$.

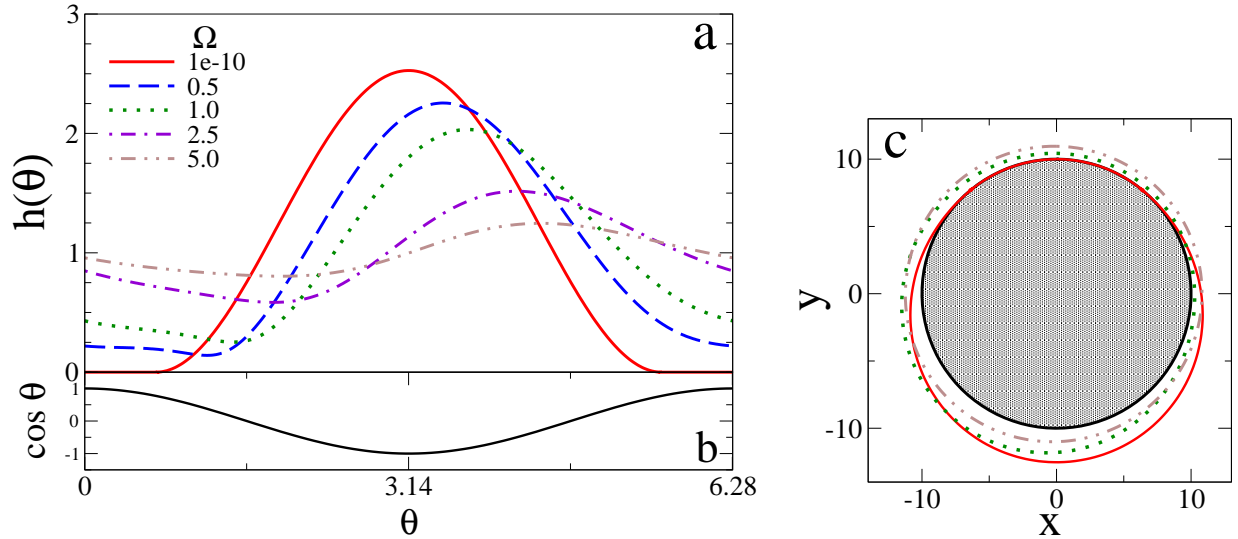


FIG. 9: Steady film thickness profiles for the case of complete wetting with $Bo = 1$ for Rotation numbers Ω as given in the legend. The remaining parameters are as in Fig. 8. Panel (a) gives the profiles as $h(\theta)$, (b) gives the space-dependent part of $\partial_h f$ (Eq. (7)), and panel (c) illustrates the profiles on a cylinder assuming a radius $R = 10$. Line styles in (c) correspond to those in (a).

Bo and increasing the rotation velocity from zero, one finds a monotonic decrease of the norm (Fig. 8) and height of the drop. Its maximum moves towards larger angular position θ , i.e., the liquid is dragged along with the rotation. However, in the wetting case there is no force besides gravity that can favour drops as compared to a flat film. As gravity acts downwards it only favours pendant drops. Therefore, the drop does not survive as a ‘coherent structure’ when dragged upwards with the rotation: it is flattened and smeared out. Typical profiles are given in Fig. 9. Note that we do not show the exact case without rotation, but choose $\Omega = 10^{-10}$ as then a dynamically created wetting layer still exists that is numerically advantageous (cf. [50]).

When increasing Ω further than shown in Fig. 8 one finds that the thickness profiles approaches a flat film. For instance, for $\text{Bo} = 1$ the norm decreases below 10^{-2} at $\Omega \approx 70$.

IV. CONCLUSION

Based on the observation that the equations in long-wave approximation that govern film flow and drop motion (i) on or in a rotating cylinder and (ii) on a heterogeneous substrate are rather similar, we have explored whether the analogy can be exploited, i.e., whether it allows results obtained for one system to be transferred to the other one. In particular, we have found that indeed for drops on a rotating cylinder there exists a counterpart of the rather involved depinning dynamics described recently for drops on heterogeneous substrates.

To study the effect we have introduced an alternative scaling. This has been necessary because the commonly used scaling contains the angular velocity of the cylinder rotation in both dimensionless parameters and in the time scale. Together with a further re-scaling of the steady state equation involving the flow rate [23, 40] this does not allow for an investigation of either the system behaviour when increasing the rotation speed of the cylinder from zero or the existence of multiple solutions for fixed rotation speed and liquid volume. The scaling employed here does allow for such studies as the rotation speed only enters a single dimensionless parameter. Furthermore, it allows us to discuss the analogy between the two systems of interest in a rather natural way. In particular, downward gravitation and rotation speed for the drop on the rotating cylinder correspond to the heterogeneous wettability and lateral driving force, respectively, for drops on heterogeneous substrates.

Guided by this analogy we have studied the behaviour of drops of partially wetting liquid

on the rotating cylinder. As a result it has been shown, how ‘switching on’ gravity (increasing the Bond number) without rotation changes the solution behaviour dramatically as the ‘gravitational heterogeneity’ along the cylinder surface effectively suppresses multidrop solutions until only the single pendant droplet underneath the cylinder survives. We have furthermore found that increasing the rotation from zero to small values, the drop is dragged along to a stable equilibrium position where downwards gravity and upwards drag compensate. At a critical speed, however, the retaining downwards force is too small and the drop is dragged above the left horizontal position. It then continuously moves with the rotating cylinder in a non-constant manner. Close to the transition the drop shows stick-slip motion. An analysis of the time-dependent behaviour has shown that the frequency related to the periodic motion goes to zero at the threshold following a power law with power $1/2$. This and the related bifurcation diagram show that the observed transition corresponds to depinning via a sniper bifurcation. The behaviour found is rather generic for the case of partial wetting. Although, here we have presented results for particular parameter values, it can be observed in a wide range of parameters, in particular, Bond number, equilibrium contact angle and wetting layer thickness. However, we have also found that the behaviour changes dramatically when strongly decreasing the equilibrium contact angle, i.e., when approaching the completely wetting case that is normally studied in the literature. When increasing the velocity of rotation in this case we have seen a transition from pendant drops underneath the cylinder to a nearly uniform film around the cylinder as [14].

The presented results indicate that it may be very fruitful to further explore the analogy of films/drops on rotating cylinders and heterogeneous substrates. We expect that the recent exploration of the three-dimensional case for depinning drops [5] and for the various transitions between ridge, drop and rivulet states [4] based on tools for the continuation of steady and stationary solutions of the two-dimensional thin film equation (physically three-dimensional system) [6] is also relevant for the case of a rotating cylinder. A future study could, e.g., elucidate the relation between the formation of azimuthal rings, pendant ridges and sets of drops.

The present circular cylinder is an analogy to a sinusoidal wettability profile. Cylinders with other cross sections, for instance, an elliptical cylinder [20] would correspond to more localised defects of the corresponding heterogeneous substrate. However, the analogue system turns out to be more complicated as a rotating non-circular cylinder introduces the aspect

of a time-periodic non-harmonic forcing parallel to the substrate into the heterogeneous substrate system.

Our equation (5) is derived under two conditions: (i) the mean (and also the maximal) film thickness has to be small as compared to the radius of the cylinder; and (ii) the local surface slope (e.g., the physical equilibrium contact angle) has to be small. Here we have assumed that the two related smallness parameters are of the same order of magnitude. In a next step one may introduce two different smallness parameters and discuss a number of distinct limits in dependence of their ratio. Such a systematic asymptotic study would also permit to discuss the influence of other effects on the depinning behaviour like, for instance, the effects of the hydrostatic pressure [1, 2], centrifugal forces [14] and inertia [19, 25].

V. ACKNOWLEDGEMENTS

I acknowledge support by the EU via grant PITN-GA-2008-214919 (MULTIFLOW). First steady state solutions were calculated by N. Barranger employing a predecessor of the present model. I benefited from discussions with E. Knobloch and several group members at Loughborough University as well as from the input of several referees and the editor.

-
- [1] ACRIVOS, A. & JIN, B. 2004 Rimming flows within a rotating horizontal cylinder: asymptotic analysis of the thin-film lubrication equations and stability of their solutions. *J. Eng. Math.* **50**, 99–120.
 - [2] ASHMORE, J., HOSOI, A. E. & STONE, H. A. 2003 The effect of surface tension on rimming flows in a partially filled rotating cylinder. *J. Fluid Mech.* **479**, 65–98.
 - [3] BAUER, C. & DIETRICH, S. 2000 Phase diagram for morphological transitions of wetting films on chemically structured substrates. *Phys. Rev. E* **61**, 1664–1669.
 - [4] BELTRAME, P., E., KNOBLOCH, HÄNGGI, P. & THIELE, U. 2010 Rayleigh and depinning instabilities of forced liquid ridges on heterogeneous substrates. *Phys. Rev. E* (submitted).
 - [5] BELTRAME, P., HÄNGGI, P. & THIELE, U. 2009 Depinning of three-dimensional drops from wettability defects. *Europhys. Lett.* **86**, 24006.

- [6] BELTRAME, P. & THIELE, U. 2010 Time integration and steady-state continuation method for lubrication equations. *SIAM J. Appl. Dyn. Syst.* **9**, 484–518.
- [7] BENOLOV, E. S., BENOLOV, M. S. & KOPTEVA, N. 2008 Steady rimming flows with surface tension. *J. Fluid Mech.* **597**, 91–118.
- [8] BENOLOV, E. S. & O'BRIEN, S. B. G. 2005 Inertial instability of a liquid film inside a rotating horizontal cylinder. *Phys. Fluids* **17**, 052106.
- [9] BONN, D., EGGERS, J., INDEKEU, J., MEUNIER, J. & ROLLEY, E. 2009 Wetting and spreading. *Rev. Mod. Phys.* **81**, 739–805.
- [10] BRANDON, S. & MARMUR, A. 1996 Simulation of contact angle hysteresis on chemically heterogeneous surfaces. *J. Colloid Interface Sci.* **183**, 351–355.
- [11] BRUSCH, L., KÜHNE, H., THIELE, U. & BÄR, M. 2002 Dewetting of thin films on heterogeneous substrates: Pinning vs. coarsening. *Phys. Rev. E* **66**, 011602.
- [12] DOEDEL, E. J., PAFFENROTH, R. C., CHAMPNEYS, A. R., FAIRGRIEVE, T. F., KUZNETSOV, Y. A., OLDEMAN, B. E., SANDSTEDTE, B. & WANG, X. J. 1997 *AUTO2000: Continuation and bifurcation software for ordinary differential equations*. Montreal: Concordia University.
- [13] DUFFY, B. R. & WILSON, S. K. 2009 Large-Biot-number non-isothermal flow of a thin film on a stationary or rotating cylinder. *Eur. Phys. J.-Spec. Top.* **166**, 147–150.
- [14] EVANS, P. L., SCHWARTZ, L. W. & ROY, R. V. 2004 Steady and unsteady solutions for coating flow on a rotating horizontal cylinder: Two-dimensional theoretical and numerical modeling. *Phys. Fluids* **16**, 2742–2756.
- [15] EVANS, P. L., SCHWARTZ, L. W. & ROY, R. V. 2005 Three-dimensional solutions for coating flow on a rotating horizontal cylinder: Theory and experiment. *Phys. Fluids* **17**, 072102.
- [16] GAU, H., HERMINGHAUS, S., LENZ, P. & LIPOWSKY, R. 1999 Liquid morphologies on structured surfaces: From microchannels to microchips. *Science* **283**, 46–49.
- [17] DE GENNES, P.-G. 1985 Wetting: Statics and dynamics. *Rev. Mod. Phys.* **57**, 827–863.
- [18] HINCH, E. J. & KELMANSON, M. A. 2003 On the decay and drift of free-surface perturbations in viscous thin-film flow exterior to a rotating cylinder. *Proc. R. Soc. London Ser. A-Math. Phys. Eng. Sci.* **459**, 1193–1213.
- [19] HOSOI, A. E. & MAHADEVAN, L. 1999 Axial instability of a free-surface front in a partially filled horizontal rotating cylinder. *Phys. Fluids* **11**, 97–106.

- [20] HUNT, R. 2008 Numerical solution of the free-surface viscous flow on a horizontal rotating elliptical cylinder. *Numer. Meth. Part Differ. Equ.* **24**, 1094–1114.
- [21] ISRAELACHVILI, J. N. 1992 *Intermolecular and Surface Forces*. London: Academic Press.
- [22] JOHN, K., HÄNGGI, P. & THIELE, U. 2008 Ratchet-driven fluid transport in bounded two-layer films of immiscible liquids. *Soft Matter* **4**, 1183–1195.
- [23] KARABUT, E. A. 2007 Two regimes of liquid film flow on a rotating cylinder. *J. Appl. Mech. Tech. Phys.* **48**, 55–64.
- [24] KARGUPTA, K. & SHARMA, A. 2003 Mesopatterning of thin liquid films by templating on chemically patterned complex substrates. *Langmuir* **19**, 5153–5163.
- [25] KELMANSON, M. A. 2009 On inertial effects in the Moffatt-Pukhnachov coating-flow problem. *J. Fluid Mech.* **633**, 327–353.
- [26] KONNUR, R., KARGUPTA, K. & SHARMA, A. 2000 Instability and morphology of thin liquid films on chemically heterogeneous substrates. *Phys. Rev. Lett.* **84**, 931–934.
- [27] LENZ, P. & LIPOWSKY, R. 2000 Stability of droplets and channels on homogeneous and structured surfaces. *Eur. Phys. J. E* **1**, 249–262.
- [28] MERKT, D., POTOTSKY, A., BESTEHORN, M. & THIELE, U. 2005 Long-wave theory of bounded two-layer films with a free liquid-liquid interface: Short- and long-time evolution. *Phys. Fluids* **17**, 064104.
- [29] MOFFATT, H. K. 1977 Behavior of a viscous film on outer surface of a rotating cylinder. *J. Mec.* **16**, 651–673.
- [30] NOAKES, C. J., KING, J. R. & RILEY, D. S. 2005 On three-dimensional stability of a uniform, rigidly rotating film on a rotating cylinder. *Q. J. Mech. Appl. Math.* **58**, 229–256.
- [31] NOAKES, C. J., KING, J. R. & RILEY, D. S. 2006 On the development of rational approximations incorporating inertial effects in coating and rimming flows: a multiple-scales approach. *Q. J. Mech. Appl. Math.* **59**, 163–190.
- [32] O’BRIEN, S. B. G. 2002 Linear stability of rimming flow. *Q. Appl. Math.* **60**, 201–211.
- [33] ORON, A., DAVIS, S. H. & BANKOFF, S. G. 1997 Long-scale evolution of thin liquid films. *Rev. Mod. Phys.* **69**, 931–980.
- [34] ORON, A. & ROSENAU, P. 1992 Formation of patterns induced by thermocapillarity and gravity. *J. Physique II France* **2**, 131–146.
- [35] PEDLEY, T. J. 1967 The stability of rotating flows with a cylindrical free surface. *J. Fluid*

- Mech.* **30**, 127–147.
- [36] PETERSON, R. C., JIMACK, P. K. & KELMANSON, M. A. 2001 On the stability of viscous free-surface flow supported by a rotating cylinder. *Proc. R. Soc. London Ser. A-Math. Phys. Eng. Sci.* **457**, 1427–1445.
- [37] PHILLIPS, O. M. 1960 Centrifugal waves. *J. Fluid Mech.* **7**, 340–352.
- [38] PISMEN, L. M. 2001 Nonlocal diffuse interface theory of thin films and the moving contact line. *Phys. Rev. E* **64**, 021603.
- [39] PISMEN, L. M. & THIELE, U. 2006 Asymptotic theory for a moving droplet driven by a wettability gradient. *Phys. Fluids* **18**, 042104.
- [40] PUKHNACHEV, V. V. 1977 The liquid film motion on the rotating cylinder surface at the presence of gravity. *Prikl. Mekh. Teor. Fiz.* **3**, 77–88.
- [41] PUKHNACHOV, V. V. 2005 On the equation of a rotating film. *Sib. Math. J.* **46**, 913–924.
- [42] QUÉRÉ, D., AZZOPARDI, M. J. & DELATTRE, L. 1998 Drops at rest on a tilted plane. *Langmuir* **14**, 2213–2216.
- [43] REISFELD, B. & BANKOFF, S. G. 1992 Nonisothermal flow of a liquid-film on a horizontal cylinder. *J. Fluid Mech.* **236**, 167–196.
- [44] ROCKFORD, L., LIU, Y., MANSKY, P., RUSSELL, T. P., YOON, M. & MOCHRIE, S. G. J. 1999 Polymers on nanoporous, heterogeneous surfaces. *Phys. Rev. Lett.* **82**, 2602–2605.
- [45] RUSCHAK, K. J. & SCRIVEN, L. E. 1976 Rimming flow of liquid in a rotating horizontal cylinder. *J. Fluid Mech.* **76**, 113–125.
- [46] SCHWARTZ, L. W. & GAROFF, S. 1985 Contact-angle hysteresis on heterogeneous surfaces. *Langmuir* **1**, 219–230.
- [47] STROGATZ, S. H. 1994 *Nonlinear Dynamics and Chaos*. Addison-Wesley.
- [48] THIELE, U. 2010 Thin film evolution equations from (evaporating) dewetting liquid layers to epitaxial growth. *J. Phys.: Condens. Matter* **22**, 084019.
- [49] THIELE, U., BRUSCH, L., BESTEHORN, M. & BÄR, M. 2003 Modelling thin-film dewetting on structured substrates and templates: Bifurcation analysis and numerical simulations. *Eur. Phys. J. E* **11**, 255–271.
- [50] THIELE, U. & KNOBLOCH, E. 2004 Thin liquid films on a slightly inclined heated plate. *Physica D* **190**, 213–248.
- [51] THIELE, U. & KNOBLOCH, E. 2006 Driven drops on heterogeneous substrates: Onset of

- sliding motion. *Phys. Rev. Lett.* **97**, 204501.
- [52] THIELE, U. & KNOBLOCH, E. 2006 On the depinning of a driven drop on a heterogeneous substrate. *New J. Phys.* **8**, 313, 1–37.
- [53] THIELE, U., VELARDE, M. G., NEUFFER, K., BESTEHORN, M. & POMEAU, Y. 2001 Sliding drops in the diffuse interface model coupled to hydrodynamics. *Phys. Rev. E* **64**, 061601.
- [54] THORODDSEN, S. T. & MAHADEVAN, L. 1997 Experimental study of coating flows in a partially-filled horizontally rotating cylinder. *Exp. Fluids* **23**, 1–13.
- [55] WEIDNER, D. E., SCHWARTZ, L. W. & ERES, M. H. 1997 Simulation of coating layer evolution and drop formation on horizontal cylinders. *J. Colloid Interface Sci.* **187**, 243–258.
- [56] YIH, C. S. & KINGMAN, J. F. C. 1960 Instability of a rotating liquid film with a free surface. *Proc R Soc London Ser A-Math* **258**, 63–89.